

An approximation of behind-casing hydraulic conductivity between layers from transient pressure analysis

Freddy Humberto Escobar ^a, Angela María Palomino ^a & Alfredo Ghisays-Ruiz ^b

^a Grupo de Investigación GIPE de la Facultad de Ingeniería, Universidad Surcolombiana, Neiva, Colombia. fescobar@usco.edu.co, angela.palomino2609@gmail.com

^b Grupo de Investigación Geología, Geofísica y Procesos Marino-Costeros, Universidad del Atlántico, Barranquilla, Colombia. alfghi1@gmail.com

Received: December 10th, 2018. Received in revised form: June 4th, 2019. Accepted: June 10th, 2019.

Abstract

Flow behind the casing has normally been identified and quantified using production logging tools. Very few applications of pressure transient analysis, which is much cheaper, have been devoted to determining compromised cemented zones. In this work, a methodology for a well test interpretation for determining conductivity behind the casing is developed. It provided good results with synthetic examples.

Keywords: radial flow; linear flow; TDS technique; pressure derivative.

Aproximación a la conductividad hidráulica de flujo detrás del revestimiento entre capas de pruebas de presión

Resumen

El flujo detrás del revestimiento se ha identificado y cuantificado normalmente utilizando herramientas de registro de producción. Se han efectuado muy pocos desarrollos de análisis de presión transitoria, que son mucho más baratas, para la determinación de zonas cementadas comprometidas. En este trabajo, se desarrolla una metodología para la interpretación de las pruebas de pozo para la determinación de la conductividad detrás del revestimiento y se prueba con buenos resultados con ejemplos sintéticos.

Palabras clave: flujo radial; flujo lineal; técnica TDS; derivada de presión.

1. Introduction

Determining cement integrity has long been a challenge in the oil industry. Production logging tools have been the most useful tools for finding compromised cement zones where cross-flow behind the casing takes place. Among these methods, [10] presented a thermal neutron log decay tool for gamma ray detection so water saturation in cased holes could be evaluated. [1] measured the acoustic behavior of flow behind pipes in commingled reservoirs with different pressures. [2] provided a radial differential temperature (RDT) logging tool to measure variations in temperature inside the casing wall affected by thermal properties and fluid movement. [6] used oxygen activation to determine water-flow velocity behind the casing.

Very few works are found for determining fluid flow behind the casing using transient pressure analysis. [5] presented some numerical simulation results to monitor flow behind the casing using the pressure derivative versus the time log-log plot. They did not quantify the amount of flow between the layers. [7] presented an excellent analytical model to quantify flow behind the casing and measure well-flowing pressure in each layer. Later, [8] used the model introduced by [7] to present some pressure derivative behavior and establish the effect of flow capacity contrast on the pressure derivative behavior in both layers. He also provided two field examples in which interpretation was performed by non-linear regression analysis.

However, an easy-to-use methodology for interpretation of pressure tests when flow behind the casing takes place does not yet exist. In this work, the model presented by [7] is

How to cite: Escobar, F.H., Palomino, A.M., and Ghisays-Ruiz, A., An approximation of behind-casing hydraulic conductivity between layers from transient pressure analysis. DYNA, 86(210), pp. 108-114, July - September, 2019.

used, so pressure derivative behaviors were studied under the three scenarios considered by [8], so unique features found on the pressure derivative plot were used and expressions for the estimation of the conductivity behind the casing were developed and successfully tested with synthetic examples. It has been demonstrated that the *TDS* technique, [9], is very practical and efficient for well-test interpretation. A summary of its use has been recently introduced by [3]. They reported many cases where the *TDS* technique, [9], provided accurate and practical results. The latest application of *TDS* Technique was devoted to horizontal wells in sensitive-stress reservoirs [4], respectively.

2. Mathematical Model

The mathematical model presented by [8] is given in the Laplacian domain as:

$$FC = \frac{k_0 A_0}{L} \quad (1)$$

$$r_{we1} = r_{w1} e^{-s_1} \quad (2)$$

$$r_{we2} = r_{w2} e^{-s_2} \quad (3)$$

$$\eta_j = \frac{0.0002637 k_j}{\phi_j \mu (c_t)_j}; j = 1, 2 \quad (4)$$

$$\alpha_j = \frac{k_j h_j (r_w)_j}{141.2 \mu}; j = 1, 2 \quad (5)$$

$$\bar{P}_{wf1}(l) = \frac{P_0}{l} \left[\frac{qB}{24Cl + \frac{\alpha_1 \sqrt{l} K_1 \left(r_{w1} \sqrt{\frac{l}{\eta_1}} \right)}{K_0 \left(r_{we1} \sqrt{\frac{l}{\eta_1}} \right)} + \frac{\alpha_2 \sqrt{l} K_1 \left(r_{w2} \sqrt{\frac{l}{\eta_2}} \right)}{K_0 \left(r_{we2} \sqrt{\frac{l}{\eta_2}} \right) + \frac{282.4 \pi \mu \alpha_2}{F_c} \sqrt{\frac{l}{\eta_2}} K_1 \left(r_{w2} \sqrt{\frac{l}{\eta_2}} \right)}} \right] \quad (6)$$

$$\beta_1 = \frac{\bar{P}_{wf1}(l) - \frac{P_0}{l}}{K_0 \left(r_{we1} \sqrt{\frac{l}{\eta_1}} \right)} \quad (7)$$

$$\beta_2 = \frac{\bar{P}_{wf1}(l) - \frac{P_0}{l}}{K_0 \left(r_{we2} \sqrt{\frac{l}{\eta_2}} \right) + \frac{282.4 \pi \mu \alpha_2}{F_c} \sqrt{\frac{l}{\eta_2}} K_1 \left(r_{w2} \sqrt{\frac{l}{\eta_2}} \right)} \quad (8)$$

$$\bar{P}_{wf2} = \frac{P_0}{l} + \beta_2 K_0 \left(r_{we2} \sqrt{\frac{l}{\eta_2}} \right) \quad (9)$$

$$\bar{q}_1 B = -\alpha_1 \beta_1 \sqrt{\frac{l}{\eta_1}} K_1 \left(r_{w1} \sqrt{\frac{l}{\eta_1}} \right) \quad (10)$$

$$\bar{q}_2 B = -\alpha_2 \beta_2 \sqrt{\frac{l}{\eta_2}} K_1 \left(r_{w2} \sqrt{\frac{l}{\eta_2}} \right) \quad (11)$$

The dimensionless parameters are defined by:

$$t_{Dj} = \frac{\eta_j t_j}{(r_w^2)_j}; j = 1, 2 \quad (12)$$

$$P_{Dj} = \frac{\alpha_j \Delta P_j}{qB(r_w^2)_j}; j = 1, 2 \quad (13)$$

$$(t_D^* P_D)_j = \frac{\alpha_j (t^* \Delta P')_j}{qB(r_w^2)_j}; j = 1, 2 \quad (14)$$

As observed from the model, the interpretation requires simultaneously recording well pressure from the two adjacent layers that are isolated along the wellbore, as depicted in Fig. 1.

3. Transient pressure behavior

Eqs. (6) and (9) provide the well-flowing pressure at layers 1 and 2 as sketched in the solution system of Fig. 1. When cement is compromised so fluid can flow behind the casing from the underlying layer (layer 2) to the producing layer (layer 1), a simultaneous effect of a radial flow regime on the horizontal plane and a linear flow regime along the vertical axes (behind the casing) is expected to develop during the middle-time flow period, as depicted in Fig. 2.

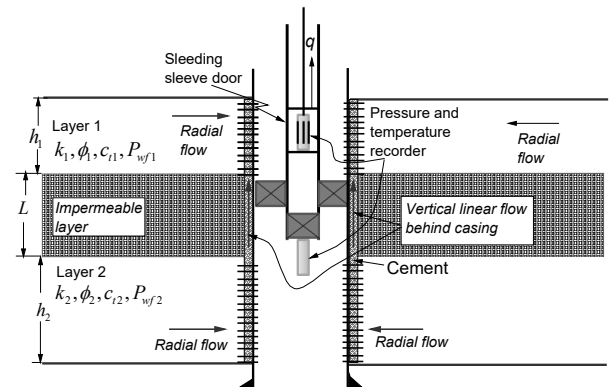


Figure 1. Schematic of solution system.
Source: The Authors.

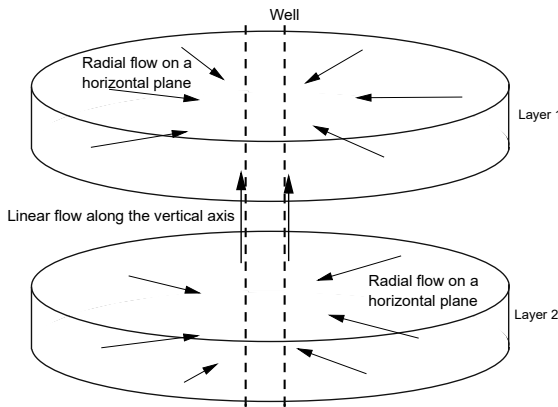


Figure 2. System flow regimes.
Source: The Authors.

This combination of the radial and linear flow regime, called here radi-linear (RL) flow regime, has a non-zero slope on the late-time of the pressure-derivative curve. The inclination of the slope is positive when flow leaves the layer and negative when the flow enters or feeds the layer.

It is also important to point out that as flow capacity or conductivity along the cement shaft change so does the slope of the pressure derivative. In other words, several values of pressure-derivative slopes can be observed leading to several mathematical flow behaviors. If a single slope was developed, the interpretation would be much easier. The pressure behavior is also a function of the flow-capacity, kh , contrast between the two layers. Therefore, there are three possible scenarios of pressure behavior depending upon the flow-capacity contrast. For instance, when $k_2h_2 > k_1h_1$ (refer to Fig. 3), the radi-linear flow regime sees conductivity values up to 200 md-ft (although shown 100 md-ft in the plot) in layer 2, and the slope of the pressure derivative is positive. For values higher than 200 md-ft, not shown in the plot, the pressure derivative becomes flat. Then, for values between 200 and 4000 md-ft, changes in the slope of the pressure derivative are observed on the producing layer (layer 1). However, the slope is negative because the layer is being fed by fluid.

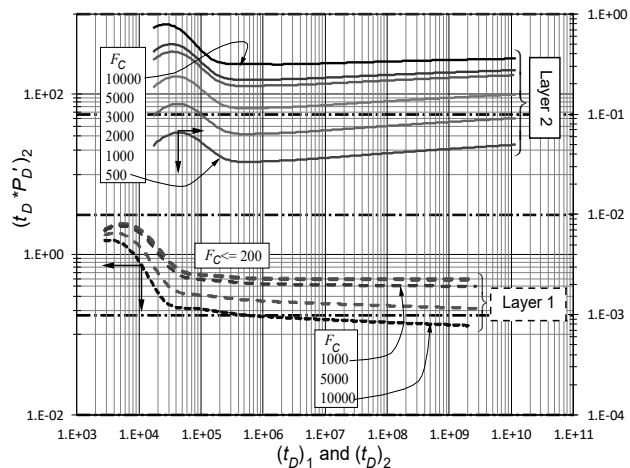


Figure 3. Dimensionless pressure derivative behavior for $k_2h_2 > k_1h_1$.
Source: The Authors.

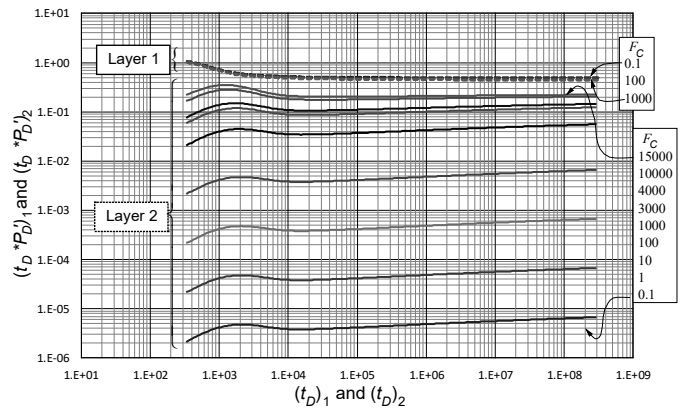


Figure 4. Dimensionless pressure derivative behavior for $k_2h_2 = k_1h_1$.
Source: The Authors.

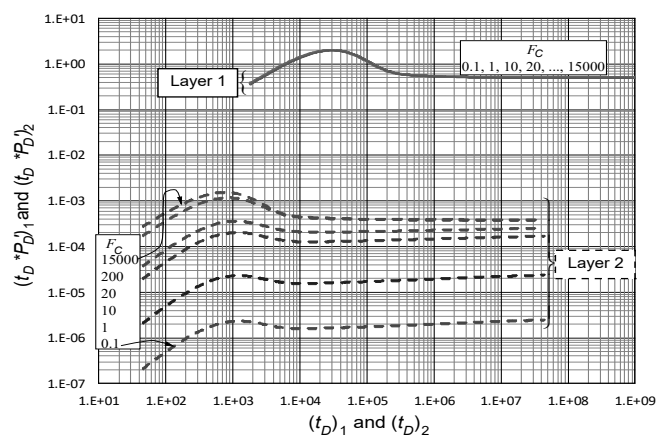


Figure 5. Dimensionless pressure derivative behavior for $k_2h_2 < k_1h_1$.
Source: The Authors.

Fig. 4 shows no contrast in flow capacity, $k_2h_2 = k_1h_1$. Layer 1 always displays a flat pressure derivative, indicating that the pressure derivative measurements of layer 1 cannot be interpreted. A positive pressure-derivative slope is observed during the middle time period. As conductivity increases, the slope of the pressure derivative slowly decreases after about 15000 md-ft. Values of conductivity greater than that provide a flat pressure derivative, so conductivity can no longer be predicted.

The last scenario considers $k_2h_2 < k_1h_1$, as reported in Fig. 5. Notice that there are no changes in the slope of the pressure derivative in layer 1 for any value of conductivity, and small changes are only observed in layer 2 for conductivity values less than 200 md-ft.

4. Pressure derivative analysis interpretation

The interpretation methodology presented here follows the philosophy of the *TDS* Technique, Tiab (1995), to develop expressions from characteristic points. In this case, the slope of the pressure derivative curve becomes the characteristic feature. As mentioned before, the slope of the pressure derivative is a function of the layers' flow capacity and the behind-casing conductivity. Then, the equations were

grouped according to an approximated-pressure derivative slope. Once flow behind the casing is suspected, the pressure derivatives from the two recorders are plotted and, depending on each scenario, the slope will determine the equation to be used.

4.1. Case 1 – $k_2h_2 > k_1h_1$

When $F_C \leq 20$ at layer 2, the average slope value for this group of conductivities is 0.0411. The following empirical expression, with a correlation coefficient of 0.999927, was obtained:

$$\frac{t_D * P_D'}{F_C} = 0.0000416 t_D^{0.0411} \tag{15}$$

After plugging in the dimensionless quantities given by Equations (11) and (14), solving for the behind-casing conductivity yields:

$$F_C = \frac{238.79 k_2 h_2 (t * \Delta P')_{RL2} \left(\frac{\phi_2 \mu c_{i2} r_{w2}^2}{k_2 t_{RL2}} \right)^{0.0411}}{q \mu B} \tag{16}$$

All the developed expressions in this work have a correlation coefficient of 0.999927. When $20 < F_C \leq 200$ at layer 2, the following fit equation was obtained:

$$\frac{t_D * P_D'}{F_C} = 0.0022147 t_D^{0.0408} \tag{17}$$

By the same token, Equation (16), it yields:

$$F_C = \left[\frac{4.64 k_2 h_2 (t * \Delta P')_{RL2} \left(\frac{\phi_2 \mu c_{i2} r_{w2}^2}{k_2 t_{RL2}} \right)^{0.0408}}{q \mu B} \right] \tag{18}$$

It is difficult to distinguish between the slopes of Equations (16) and (18). However, it is recommended

A fit equation, with a correlation coefficient of -1, for $200 < F_C \leq 3000$ at layer 1 was obtained:

$$\frac{t_D * P_D'}{F_C^{-0.17}} = \frac{1.5255}{t_D^{0.0083}} \tag{19}$$

Replacing the dimensionless quantities and solving for the conductivity yielded,

$$F_C = \left[\frac{201.12 q \mu B}{k_1 h_1 (t * \Delta P')_{RL1} \left(\frac{\phi_1 \mu c_{i1} r_{w1}^2}{k_1 t_{RL1}} \right)^{0.0083}} \right]^{-1/0.17} \tag{20}$$

A fit equation, with a correlation coefficient of 0.9999, for $3000 < F_C \leq 5000$ at layer 1 also gave:

$$F_C^{0.5} (t_D * P_D') = \frac{23.8283}{t_D^{0.01971}} \tag{21}$$

After replacing the dimensionless quantities for layer 1 given by Equations (12) and (14), the following expression was obtained:

$$F_C = \left[\frac{3597.924 q \mu B}{k_1 h_1 (t * \Delta P')_{RL1} \left(\frac{\phi_1 \mu c_{i1} r_{w1}^2}{k_1 t_{RL1}} \right)^{0.01971}} \right]^2 \tag{22}$$

4.2. Case 2 – $k_2h_2 = k_1h_1$

Since the pressure derivative at layer 1 does not register any change, all the expressions were developed following the same procedure used in case 1 only for layer 2 in order to obtain conductivity expressions:

when $F_C \leq 200$, the correlation coefficient is 0.99994, and the obtained fitted expression is:

$$\frac{t_D * P_D'}{F_C^{0.996}} = 0.0000244 t_D^{0.052} \tag{23}$$

$$F_C = \left[\frac{445.308 k_2 h_2 (t * \Delta P')_{RL2} \left(\frac{\phi_2 \mu c_{i2} r_{w2}^2}{k_2 t_{RL2}} \right)^{0.052}}{q \mu B} \right]^{1/0.996} \tag{24}$$

The correlation coefficient is 0.999929 for $200 < F_C \leq 1000$, and the fitted expression is:

$$\frac{t_D * P_D'}{F_C^{0.6}} = 0.000293 t_D^{0.047} \tag{25}$$

$$F_C = \left[\frac{35.577 k_2 h_2 (t * \Delta P')_{RL2} \left(\frac{\phi_2 \mu c_{i2} r_{w2}^2}{k_2 t_{RL2}} \right)^{0.047}}{q \mu B} \right]^{1/0.6} \tag{26}$$

For $1000 < F_C \leq 4000$, the correlation coefficient is 0.99988 and the fit is:

$$\frac{t_D * P_D'}{[\log(F_C)]^5} = 0.000131 t_D^{0.032} \tag{27}$$

$$[\log(F_C)]^5 = \left[\frac{k_2 h_2 (t * \Delta P')_{RL2} \left(\frac{\phi_2 \mu c_{i2} r_{w2}^2}{k_2 t_{RL2}} \right)^{0.032}}{70.32 q \mu B} \right] \tag{28}$$

A correlation coefficient of 0.99984 was found for $4000 < F_C \leq 7000$, the fit is given by;

$$\frac{t_D * P_D'}{F_C^{0.45}} = 0.002194 t_D^{0.024} \tag{29}$$

$$F_C = \left[\frac{3.9253k_2h_2(t^* \Delta P')_{RL2}}{q\mu B} \left(\frac{\phi_2 \mu c_{t2} r_w^2}{k_2 t_{RL2}} \right)^{0.024} \right]^{1/0.45} \quad (30)$$

For $7000 < F_C \leq 15000$, the correlation coefficient is 0.99975

$$\frac{t_D^* P_D'}{F_C^{0.25}} = 0.0119 t_D^{0.0137} \quad (31)$$

$$F_C = \left[\frac{k_2 h_2 (t^* \Delta P')_{RL2}}{1.5018 q \mu B} \left(\frac{\phi_2 \mu c_{t2} r_w^2}{k_2 t_{RL2}} \right)^{0.014} \right]^{1/0.28} \quad (32)$$

4.3. Case 3 – $k_2 h_2 < k_1 h_1$

Because only pressure-derivative changes were presented at layer 2, only expressions for this layer were developed:

For $F_C \leq 1$, $R^2 = 0.999908$,

$$\frac{t_D^* P_D'}{F_C} = \frac{t_D^{0.0513}}{99985.195} \quad (33)$$

$$F_C = \frac{1084.25 k_2 h_2 (t^* \Delta P')_{RL2}}{q \mu B} \left(\frac{\phi_2 \mu c_{t2} r_w^2}{k_2 t_{RL2}} \right)^{0.0517} \quad (34)$$

For $1 < F_C \leq 10$, $R^2 = 0.999998$,

$$\frac{t_D^* P_D'}{F_C^{0.85}} = \frac{t_D^{0.038}}{77732.289} \quad (35)$$

$$F_C = \left[\frac{752.95 k_2 h_2 (t^* \Delta P')_{RL2}}{q \mu B} \left(\frac{\phi_2 \mu c_{t2} r_w^2}{k_2 t_{RL2}} \right)^{0.038} \right]^{1/0.85} \quad (36)$$

For $10 < F_C \leq 20$,

$$\frac{t_D^* P_D'}{F_C^{0.7}} = \frac{t_D^{0.026}}{49340.213} \quad (37)$$

$$F_C = \left[\frac{432.93 k_2 h_2 (t^* \Delta P')_{RL2}}{q \mu B} \left(\frac{\phi_2 \mu c_{t2} r_w^2}{k_2 t_{RL2}} \right)^{0.026} \right]^{1/0.7} \quad (38)$$

When the pressure-derivative data present noise, it is recommended to draw a line throughout the points of interest (along the radi-linear flow regime) and to read the value of the pressure derivative at the time of 1 hr. An average value is then obtained, and the expression is easier to use. For instance, Equation (38) will become:

$$F_C = \left[\frac{432.93 k_2 h_2 (t^* \Delta P')_{RL2}}{q \mu B} \left(\frac{\phi_2 \mu c_{t2} r_w^2}{k_2} \right)^{0.026} \right]^{1/0.7} \quad (39)$$

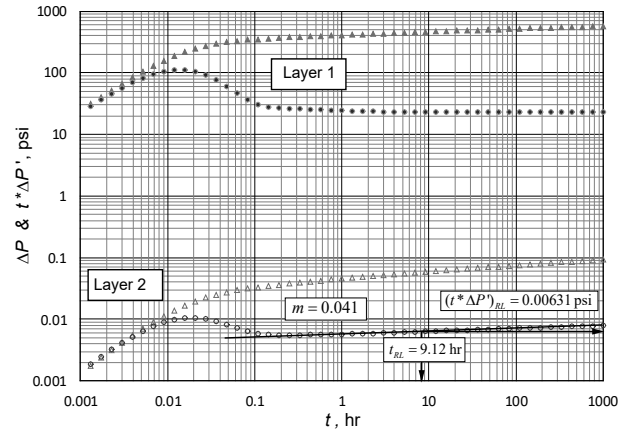


Figure 6. Pressure and pressure derivative versus time log-log plot for example 5.1, $k_2 h_2 > k_1 h_1$. Source: The Authors

5. Examples

[8] provided two field examples. However, most reservoir and fluid information is incomplete, making it impossible to provide actual field data. Therefore, only synthetic examples are provided.

5.1. Synthetic example 1

Using the information, a simulated test was performed by [7] for a case where the flow capacity of the layer 2 was greater than that of layer 1. Data used for the simulation is given in the second column of Table 1. Pressure and pressure derivative versus time are provided in Fig. 6. Find the conductivity behind the casing.

Solution. The below information was obtained from Fig.

6.

$$t_{RL2} = 9.12 \text{ hr} \quad (t^* \Delta P')_{RL2} = 0.00631 \text{ psi} \quad m = 0.041$$

Because the closest slope corresponds to Equation (16), this expression is used to estimate the conductivity:

$$F_C = \frac{238.79(2200)(100)(0.00631)}{(900)(5)(1.35)} \left(\frac{(0.18)(5)(3 \times 10^{-6})(0.3^2)}{2200(9.12)} \right)^{0.0411} = 20.36 \text{ md-ft}$$

5.2. Synthetic example 2

Another synthetic example for equal flow-capacity layers was run with data from the third column of Table 1. Pressure and pressure derivative data versus time data are plotted in Fig. 7.

Solution. The below information was obtained from Fig. 7. Equation (24) is used since the closest slope is 0.047.

$$t_{RL} = 110 \text{ hr} \quad (t^* \Delta P')_{RL2} = 0.0000195 \text{ psi} \quad m = 0.052$$

$$F_C = \left[\frac{445.308(300)(80)(0.292)}{(500)(1)(1.1)} \left(\frac{(0.2)(1)(1 \times 10^{-5})(0.35^2)}{(300)(110)} \right)^{0.047} \right]^{1/0.9} = 0.0996 \text{ md-ft}$$

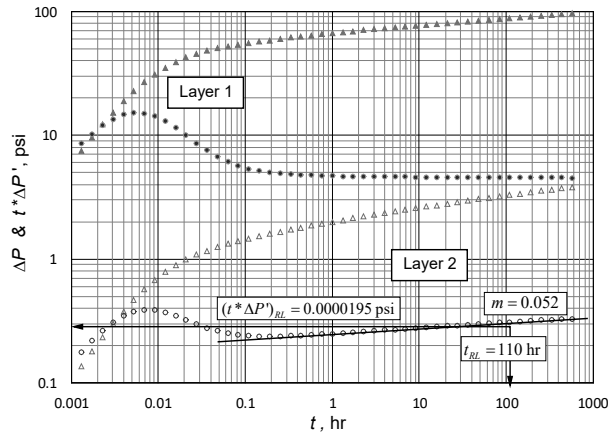


Figure 7. Pressure and pressure derivative versus time log-log plot for example 5.2, $k_2h_2 = k_1h_1$. Source: The Authors.

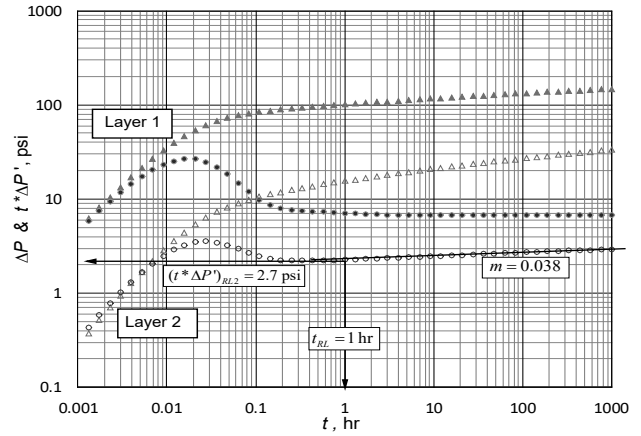


Figure 8. Pressure and pressure derivative versus time log-log plot for example 5.3, $k_2h_2 < k_1h_1$. Source: The Authors.

Table 1. Reservoir and fluid data for examples.

PARAMETER	Example 1	Example 2	Example 3
k_1 , md	440	300	800
k_2 , md	2200	300	5
ϕ_1 , %	22	20	5
ϕ_2 , %	18	20	5
c_{11} , 1/psi	3×10^{-6}	1×10^{-5}	1×10^{-6}
c_{22} , 1/psi	3×10^{-6}	1×10^{-5}	1×10^{-6}
h_1 , ft	42	80	80
h_2 , ft	100	80	10
r_{w1} , ft	0.3	0.35	0.35
r_{w2} , ft	0.3	0.35	0.35
s_1	2	0	2
s_2	-0	0	2
F_C , md-ft	20	0.1	10
q , bbl/D	900	500	900
B , rb/STB	1.35	1.15	1.35
μ , cp	5	1	5
C , bbl/psi	0.002	0.005	0.01
P_b , psi	5300	5780	4300
Abs. error, %	1.76	0.4	3.6

Source: The Authors.

5.3. Synthetic example 3

This simulated example was run with data from the fourth column of Table 1 for a case when the flow capacity of layer 1 is greater than the flow capacity of layer 2. Pressure and pressure derivative data versus time data are reported in Fig. 8.

Solution. The following information was read from Fig. 8.

$$(t^* \Delta P')_{RL2} = 2.27 \text{ psi} \quad m = 0.038$$

Notice that the found slope leads to using Equation (36) but at a time of 1 hr, so that:

$$F_C = \left[\frac{752.95(5)(10)(2.27)}{(900)(5)(1.35)} \right]^{1/0.85} \left(\frac{(0.05)(5)(1 \times 10^{-6})(0.35^2)}{5} \right)^{0.038} = 9.64 \text{ md-ft}$$

6. Comments on the results

As observed, a classification of three cases was performed depending upon the contrast in flow capacity: a) layer 1 has higher flow capacity than layer 2, b) layer 1 has lower flow capacity than layer 1, and c) both layers have same flow capacity. Therefore, one example is presented for each case. Although, [8] presents several examples of actual field data concerning flow behind the casing, they do not supply additional information of fluid, well and reservoir parameters, then, it was not possible to test the formulated methodology with a real field example. In all the synthetic examples the value of estimated hydraulic conductivity of the cement behind the casing provided very well results compared to the initially assumed values for the simulations: 20, 0.1 and 10 md-ft for examples 1, 2 and 3, respectively. In the worked examples, the obtained conductivity values match well with those used as input data. The absolute deviation errors were 1.76, 0.4 and 3.6%, as reported in Table 1, which are very well acceptable values in well test analysis.

7. Conclusions

1. Expressions for determining the conductivity behind the casing were developed and successfully tested with simulated examples that gave good results in estimating the conductivity. These expressions are ranged with the value of the slope of the pressure derivative curve during the middle time period.
2. The combination of the horizontal radial flow regime and the vertical linear flow regime behind the casing provides a singular effect on the pressure derivative reflected by a non-zero slope during the middle time period. This combine effect was called here the radi-linear flow regime, and it takes a positive value when the flow leaves the layer and a negative value when the flow feeds the layer.
3. The contrast in flow capacity between the layers and the change in conductivity along the compromised zone

behind the casing causes the pressure derivative slope to change its slope during the middle time period.

4. Care must be taken while estimating the slope, which is very sensitive, and for noisy data it is recommended to draw a line over the radi-linear flow and read the pressure derivative value at 1 hr.

Nomenclature

B	Volume factor, rb/STB
C	Wellbore storage coefficient, bbl/psi
c_t	Total system compressibility, psi ⁻¹
F_C	Hydraulic conductivity of channel behind casing, md-ft
k	Reservoir horizontal permeability, md
h	Reservoir thickness, ft
kh	Reservoir flow capacity, md-ft
K_0	Bessel function
K_1	Bessel function
l	Laplace operator
m	Slope
P	Pressure, psi
P_D	Dimensionless pressure
P_i	Initial reservoir pressure, psi
P_{wf}	Wellbore flowing pressure, psi
q	Liquid flow rate, BPD
r_w	Wellbore radius, ft.
r_{we}	Effective wellbore radius, ft.
s	Skin factor
t	Time, hr
t_D	Dimensionless time
$t_D^*P_D'$	Dimensionless pressure derivative
$(t^*\Delta P')$	Pressure derivative, psi

Greeks Symbols

α	Layer flow parameter, md-ft ² /cp
ϕ	Porosity, fraction
η	Layer hydraulic diffusivity, md-psi/cp
μ	Viscosity, cp

Suffices

1	Referred to layer 1
2	Referred to layer 2
D	Dimensionless
i	Initial
RL	Radi-linear Flow
$RL1$	Radi-linear Flow at layer 1
$RL2$	Radi-linear Flow at layer 2
$RL1_1$	Radi-linear Flow at layer 1 at a time of 1 hr
$RL2_1$	Radi-linear Flow at layer 2 at a time of 1 hr
wf	Well flowing

References

- [1] Bakulin, A. and Korneev, V., Acoustic signatures of cross-flow behind casing: downhole monitoring experiment at teapot dome. Society of Exploration Geophysicists. DOI: 10.1190/1.2792430. Jan. 2001.
- [2] Cooke, C.E., Radial Differential Temperature (RDT) logging - A new tool for detecting and treating flow behind casing. Society of Petroleum Engineers. DOI: 10.2118/7558-PA. Jun. 1979.
- [3] Escobar, F.H., Jongkittnarukom, K. and Hernandez, C.M., The power of TDS technique for well test interpretation: a short review. Journal of Petroleum Exploration and Production Technology, 9(1), pp. 731-752, 2019. ISSN 2190-0566. DOI: 10.1007/s13202-018-0517-5. 2018.
- [4] Escobar, F.H., Zhao, Y.L., Urazan, C. and Trujillo, C.M., Pressure and pressure derivative interpretation for horizontal wells in compressible formations. Journal of Geophysics and Engineering, 15, pp. 1551-1560, 2018. ISBN 1742-2140. DOI: 10.1088/1742-2140/aaadc9. 2018.
- [5] Kremenetskiy, M.I., Ipatov, A.I. and Kokurina, V., Well-test interpretation in case of behind-the-casing crossflow. Society of Petroleum Engineers. In: SPE Russian Oil and Gas Technical Conference and Exhibition, 28-30 October, Moscow, Russia, 2008. DOI: 10.2118/115323-MS. Jan. 2008.
- [6] McKeon, D.C., Scott, H.D., Olesen, J.-R., Patton, G.L. and Mitchell, R.J., Improved oxygen-activation method for determining water flow behind casing. Society of Petroleum Engineers, 6(03), 1991. DOI: 10.2118/20586-PA
- [7] Rahman, N.M.A., Measuring behind casing hydraulic conductivity between reservoir layers. US patent and Trademark Office. Patent Application Number 14/182.430. 2014.
- [8] Rahman, N.M.A., Bin-Akresh, S.A. and Al-Thawad, F.M., Diagnosis and characterization of cross flow behind casing from transient-pressure tests. Society of Petroleum Engineers. In: SPE Annual Technical Conference and Exhibition, 28-30 September, Houston, Texas, USA, 2015. DOI: 10.2118/174999-MS
- [9] Tiab, D., Analysis of pressure and pressure derivative without type-curve matching: 1- skin and wellbore storage. Journal of Petroleum Science and Engineering, 12, pp. 171-181, 1995. DOI: 10.1016/0920-4105(95)00064-X
- [10] Wahl, J.S., Nelligan, W.B., Frentrup, A.H., Johnstone, C.W. and Schwartz, R.J., The thermal neutron decay time log. Society of Petroleum Engineers Journal, 10(04), 1970. DOI: 10.2118/2252-PA

F.H. Escobar, is a BSc. in Petroleum Engineer from Universidad de América in Bogotá, Colombia. He also holds MSc. and PhD degrees in Petroleum Engineering, both from the University of Oklahoma, USA. He is a professor of the Petroleum Engineering Department in Universidad Surcolombiana, Neiva, and he is also director of the research group, GIPE (Geoscience, Infrastructure, Productivity and Environment) in the Engineering College of Universidad Surcolombiana, Neiva, Colombia. ORCID: 0000-0003-4901-6057

A.M. Palomino, is a senior student of the Petroleum Engineering Department in Universidad Surcolombiana, Neiva, Colombia. She is a member of the research group GIPE in the Universidad Surcolombiana, Neiva, Colombia. ORCID: 0000-0001-5556-8240

A. Ghisays-Ruiz, is a BSc. in Physics from Universidad Pedagógica Nacional and a MSc in Geophysics from Universidad Nacional de Colombia. He is an associate professor at Universidad del Atlántico, Colombia, where he is also a member of the research group in Geología, Geofísica y Procesos Marino-Costeros. ORCID: 0000-0002-2927-6698